Water Mass Transformation and Subduction in the South Atlantic

J. DONNERS, S. S. DRIJFHOUT, AND W. HAZELEGER

Royal Netherlands Meteorological Institute, De Bilt, Netherlands

(Manuscript received 17 February 2004, in final form 28 January 2005)

ABSTRACT

The transformation of water masses induced by air–sea fluxes in the South Atlantic Ocean is calculated with a global ocean model, Ocean Circulation and Climate Advanced Modeling (OCCAM), and has been compared with several observational datasets. Air–sea interaction supplies buoyancy to the ocean at almost all density levels. The uncertainty of the estimates of water mass transformations is at least 10 Sv (Sv $\equiv 10^6$ $m^3\ s^{-1}$), largely caused by the uncertainties in heat fluxes. Further analysis of the buoyancy budget of the mixed layer in the OCCAM model shows that diffusion extracts buoyancy from the water column at all densities. In agreement with observations, water mass formation of surface water by air–sea interaction is completely balanced by consumption from diffusion. There is a large interocean exchange with the Indian and Pacific Oceans. Intermediate water is imported from the Pacific, and light surface water is imported from the Indian Ocean. South Atlantic Central Water and denser water masses are exported to the Indian Ocean. The air–sea formation rate is only a qualitative estimate of the sum of subduction and interocean exchange. Subduction generates teleconnections between the South Atlantic and remote areas where these water masses reemerge in the mixed layer. Therefore, the subduction is analyzed with a Lagrangian trajectory analysis. Surface water obducts in the South Atlantic, while all other water masses experience net subduction. The subducted Antarctic Intermediate Water and Subantarctic Mode Water reemerge mainly in the Antarctic Circumpolar Current farther downstream. Lighter waters reemerge in the eastern tropical Atlantic. As a result, the extratropical South Atlantic has a strong link with the tropical Atlantic basin and only a weak direct link with the extratropical North Atlantic. The impact of the South Atlantic on the upper branch of the thermohaline circulation is indirect: water is significantly transformed by air–sea fluxes and mixing in the South Atlantic, but most of it reemerges and subducts again farther downstream.

1. Introduction

The South Atlantic Ocean basin has both strong, local air–sea interaction of heat and freshwater and large interocean exchange with adjacent basins. These air–sea interaction processes cause water mass transformations in the South Atlantic, with a possibly large remote impact on the ocean circulation in other basins (Sloyan and Rintoul 2001; Karstensen and Quadfasel 2002b). Because of the thermohaline circulation (THC), the South Atlantic exports about 15 Sv (Sv $\equiv 10^6$ $m^3\ s^{-1}$) of North Atlantic Deep Water (NADW). This requires a compensating flow toward the North Atlantic at other levels. The water masses that make up the return flow are modified within the South Atlantic basin with potential impacts on the THC (Weijer et al. 2002). In this article we discuss the effects of mixing and surface buoyancy fluxes of heat and freshwater on the volume and buoyancy balance of the South Atlantic mixed layer. Furthermore, with Lagrangian analysis, the impact of water mass modification in the South Atlantic on the THC is estimated.

Two distinct methods are available to analyze the impact of mixed layer processes on the ocean circulation. First, the oceanic circulation induced by the thermal surface fluxes has been quantified by Walin (1982). He combined the ocean state with air–sea fluxes of heat to estimate the oceanic "Hadley cell." With an extension of this theory (Tziperman 1986) net sources and sinks of specific water masses can be calculated from the combination of heat and freshwater fluxes and sea surface salinity and temperature. The change of density of seawater due to surface fluxes is called water mass transformation (WMT). The convergence of water

Corresponding author address: J. Donners, The Earth Simulator Center, Japan Agency for Marine-Earth Science and Technology, Kanazawa-ku, Yokohama, Japan.
E-mail: j.donners@reading.ac.uk

within a specific density interval due to WMT is called water mass formation. Water mass transformation rates have been calculated for the North Atlantic (Speer and Tziperman 1992) and the global ocean (Speer et al. 1995).

Second, a kinematic approach can be used to estimate the exchange between the mixed layer and the underlying stratum and to assess the impact of surface processes on the internal ocean. In winter the mixed layer deepens, and, consequently, mass is transferred from the ocean interior into the mixed layer. This process, caused mostly by turbulent mixing at the mixed layer base, is called entrainment. Water masses are transformed by air–sea fluxes and mixing in the surface mixed layer. When the upper ocean restratifies in spring, the mixed layer shallows. Detrainment is the process where water masses leave the turbulent mixed layer and enter the interior ocean. After detrainment, the water masses move largely adiabatically within the interior ocean. Subduction is a fraction of the detrained mass flux: it refers to that part of the detrained water mass that is not entrained in the next winter (Cushman-Roisin 1987). The opposite process is sometimes referred to as obduction. The physics involved in subduction and obduction, however, are completely different.

In a closed basin and in steady state, the mixed layer is in a balance among transport across the winter mixed layer base, the water mass formation by air–sea fluxes, and mixing. This mixing within and across the winter mixed layer has been studied extensively by Nurser et al. (1999). In general, mixing counteracts water mass transformation by air–sea fluxes.

Marshall et al. (1999) combined WMT and subduction into one theoretical framework and analyzed the total mass balance of the water volume delimited by the winter mixed layer depth. It was shown that mixing is important everywhere and that subduction and WMT cannot easily be equated. Karstensen and Quadfasel (2002a) compared WMT rates with subduction rates for the three ocean basins of the Southern Hemisphere using observational and reanalysis data. They concluded that 13 Sv of newly formed water within the South Atlantic mixed layer is exported toward the Indian Ocean before it subducts into the interior.

Most studies on subduction and WMT concentrate on the North Atlantic or show a globally averaged picture. The aim of this study is to show WMT and subduction within the South Atlantic. The South Atlantic is a data sparse region and we therefore compare WMT rates deduced from different datasets. This gives an indication of the errors involved in the air–sea flux estimates across the South Atlantic (Sterl 2001). From observational datasets of Ekman pumping and wind stress, Lagrangian trajectories can be calculated via the Sverdrup balance. These can be used to calculate subduction and obduction rates (Qiu and Huang 1995). This approach, however, is not easily implemented for the Southern Hemisphere since it is not straightforward to apply the Sverdrup balance to the Antarctic Circumpolar Current (Gnanadesikan and Hallberg 2000). Therefore, we study subduction in more detail with a Lagrangian trajectory analysis (Döös 1995) of the Ocean Circulation and Climate Advanced Modeling (OCCAM) project (Webb et al. 1997). The Lagrangian connection of subduction and obduction areas shows the oceanic teleconnections of the South Atlantic. This enables us to estimate the influence of subduction in the South Atlantic on the global ocean. In particular, we estimate the Lagrangian connection of the South Atlantic subtropical water masses with the tropical Atlantic. Also, the routes of subducted subantarctic mode and intermediate waters are determined, which are mostly limited to the ACC. The Lagrangian connections are qualitatively compared with results from chemical tracer analyses. A detailed buoyancy analysis of the mixed layer shows the relative importance of WMT, mixing, interocean exchange, and subduction.

The paper is set up as follows: the next section introduces the theoretical framework of WMT and subduction. In section 3 the water mass transformations calculated from different datasets are discussed. Section 4 shows the buoyancy budget of the South Atlantic for the OCCAM model. Section 5 treats the Lagrangian view of the water subducted within the South Atlantic. Section 6 contains the discussion and conclusions.

2. Theoretical framework

Air–sea fluxes of heat and freshwater cause a change of buoyancy (or, equivalently, density) of ocean water directly at the surface. Because of advection and mixing processes in the surface mixed layer, this buoyancy change is carried farther down into the interior ocean. The dynamical balance of the ocean determines how the ocean water is carried farther below the mixed layer.

The volume and buoyancy balances of the mixed layer connect the kinematic and thermodynamic processes within the mixed layer. In this section we show the links among the different processes of surface forcing of heat and freshwater fluxes, the subduction process, the exchange of water with adjacent ocean basins, and diffusion.

In Fig. 1 the framework is drawn that shows the relation among air–sea transformation, subduction, and mixing. The framework is based on both Marshall et al.

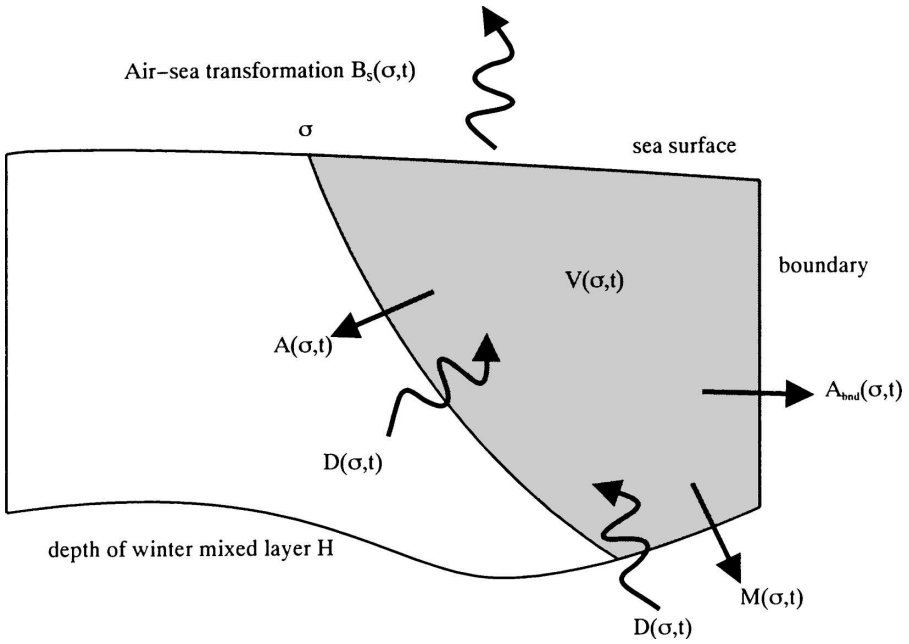

FIG. 1. Schematic diagram of the relation among air–sea transformation, diffusion, and subduction within an open-ocean region. The gray area is bounded by the horizontal region R, the sea surface, the isopycnal σ, and the depth of the winter mixed layer. The arrows point in the direction for which the quantity is defined positive.

(1999) and Walin (1982). Symbols used throughout the article are listed in the appendix.

The potential density anomaly σ is referenced to the surface pressure. Note that V, A_{bnd}, M, B, B_s, and D are quantities integrated over all densities lower than σ, while A is a volume flux across the isopycnal σ. The volume balance of V can be stated as follows:

$$\frac{\partial V(\sigma, t)}{\partial t} = -A(\sigma, t) - A_{\text{bnd}}(\sigma, t) - M(\sigma, t). \quad (1)$$

The freshwater loss due to evaporation and precipitation in the South Atlantic of the OCCAM model is 0.5 Sv and can be neglected for the volume balance. However, evaporation and precipitation is included in the buoyancy forcing $F(\sigma, t)$. If we assume that the ocean is in a steady state and that the transport through the boundaries A_{bnd} is small or known, the net advective diapycnal flux $A(\sigma, t)$ can be equated to $M(\sigma, t)$. The volume flux $M(\sigma, t)$ represents the annual mean mass flux across the deepest mixed layer:

$$M(\sigma, t) = M_{\text{Eul}}(\sigma, t) = \int\int [-\mathbf{u}_H \cdot \nabla H(x, y) - \mathbf{w}_H]\, dx\, dy, \quad (2)$$

with $\mathbf{u}_H$ the two-dimensional annual mean velocity field at the depth H. The vertical velocity at depth H is represented by $\mathbf{w}_H$. The two-dimensional integral includes all locations with a density lower than σ. Because M is the volume flux through a fixed surface, it is an Eulerian quantity. The transformation caused by mixing below the mixed layer in summer is assumed to be small in comparison with the vigorous mixing within the mixed layer and the entrainment. Therefore we took the deepest mixed layer depth as a control volume. Note that M_{Eul} could be both positive and negative. The sum of the fluxes through the winter mixed layer base from V is defined as the Eulerian subduction S_{Eul}. The sum of the fluxes into V is defined as Eulerian obduction O_{Eul}. Equation (2) has been used by Marshall et al. (1993) in their data analysis of net subduction in the North Atlantic.

The subduction process, however, is a quantity with a Lagrangian definition (Cushman-Roisin 1987). Water is subducted if it does not reenter the mixed layer during deepening of the mixed layer in the following year. We denote this Lagrangian quantity with S_{Lag}. Water that enters the mixed layer, after remaining below the mixed layer for more than one year, has been obducted (O_{Lag}). To determine if water particles resided longer than one year within the interior ocean, a Lagrangian trajectory calculation is needed. The Lagrangian net subduction M_{Lag} is the sum of Lagrangian subduction and obduction.

The Eulerian and Lagrangian subductions are in general not equal. Not all the water that enters V through the mixed layer base has resided below the mixed layer for more than one year, and some of the water that leaves V could reenter the mixed layer within a year. Another discrepancy is the change in time of the ocean circulation. While the Eulerian subduction is an annually averaged quantity across a fixed surface, the Lagrangian subduction depends on the time-varying ocean circulation along the path after the water has left the mixed layer.

The volume balance of the control volume V relates the diapycnal fluxes $A(\sigma, t)$ to the fluxes through the side and bottom boundaries of V. So far, only kinematics has been used to derive this relation. However, the diapycnal volume flux $A(\sigma, t)$ is closely connected to the buoyancy budget of V. To show this relation, we first write down the buoyancy budget (or equivalently, mass budget) for V:

$$\int_{-\infty}^{\sigma} \sigma' \frac{\partial^2 V(\sigma', t)}{\partial \sigma' \partial t} d\sigma' = -\sigma A(\sigma, t) - \int_{-\infty}^{\sigma} \sigma' \frac{\partial [A_{\text{bnd}}(\sigma', t) + M(\sigma', t)]}{\partial \sigma'} d\sigma' + B(\sigma, t). \quad (3)$$

The buoyancy balance [Eq. (3)] has a similar form as the volume balance [Eq. (1)], because mass fluxes are equal to volume fluxes times the density. The quantity σA is the advective diapycnal mass flux across the isopycnal σ. The other terms—V, A_{bnd}, and M—need to be integrated for all densities lower than σ. The buoyancy term B appears in the buoyancy budget, and not in the volume budget, because the density of water is changed without a volume flux. If we calculate the derivative to σ of both the volume [Eq. (1)] and the mass balance [Eq. (3)], we get

$$\frac{\partial^2 V}{\partial \sigma \partial t} = -\frac{\partial A}{\partial \sigma} - \frac{\partial A_{\text{bnd}}}{\partial \sigma} - \frac{\partial M}{\partial \sigma} \quad \text{and} \quad (4)$$

$$\sigma \frac{\partial^2 V}{\partial \sigma \partial t} = -A - \sigma \frac{\partial A}{\partial \sigma} - \sigma \frac{\partial A_{\text{bnd}}}{\partial \sigma} - \sigma \frac{\partial M}{\partial \sigma} + \frac{\partial B}{\partial \sigma}. \quad (5)$$

Multiplying Eq. (4) by σ and subtracting from Eq. (5) gives

$$A(\sigma, t) = \frac{\partial B(\sigma, t)}{\partial \sigma}. \quad (6)$$

The total nonadvective supply of buoyancy to V can be written as follows:

$$B(\sigma, t) = -\int_{V(\sigma,t)} \nabla \cdot \mathbf{N}_\sigma \, dV, \quad (7)$$

with $\mathbf{N}_\sigma$ the nonadvective flux of potential density. If we ignore internal sources of buoyancy like cabbeling, $B(\sigma, t)$ can be calculated from the integral of the buoyancy flux across the boundary of $V(\sigma, t)$. This buoyancy supply can be divided into two distinct components: internal diffusion processes $D(\sigma, t)$ and buoyancy fluxes through the surface $B_s(\sigma, t)$:

$$B = B_S - D, \quad (8)$$

$$D = \int\int \mathbf{N}_\sigma \cdot \mathbf{n} \, dA_1, \quad \text{and} \quad (9)$$

$$B_S = \int\int \left[\frac{\alpha}{C_w} Q + \rho_0 \beta S (E - P) \right] dA_2, \quad (10)$$

with A_1 and A_2 the surfaces that enclose the control volume $V(\sigma, t)$ respectively below and at the sea surface. The coefficients α and β represent the thermal expansion and haline contraction of seawater. The quantities Q and $(E - P)$ are the heat and freshwater fluxes from the atmosphere to the ocean. The quantity c_w is the specific heat of seawater and S is the sea surface salinity. The transformation of seawater by air–sea fluxes is separately defined as F:

$$F(\sigma, t) = \frac{\partial B_s(\sigma, t)}{\partial \sigma}. \quad (11)$$

The diapycnal fluxes $A(\sigma, t)$ are difficult to measure in the ocean. However, the diapycnal fluxes within the mixed layer can be eliminated from the balance if we combine Eqs. (1) and (6):

$$\frac{\partial V}{\partial t} = -F + \frac{\partial D}{\partial \sigma} - A_{\text{bnd}} - M. \quad (12)$$

Water masses in oceanography are normally labeled by a specific density interval. To analyze the balance of a water mass defined by two isopycnals σ_1 and σ_2, we have to subtract the integrated balance for these two isopycnal levels:

$$\frac{\partial [V(\sigma_2) - V(\sigma_1)]}{\partial t} = -F(\sigma_2) + F(\sigma_1) + \frac{\partial [D(\sigma_2) - D(\sigma_1)]}{\partial \sigma} - A_{\text{bnd}}(\sigma_2) + A_{\text{bnd}}(\sigma_1) - M(\sigma_2) + M(\sigma_1). \quad (13)$$

In section 3 we compare the transformation by air–sea fluxes $F(\sigma, t)$ calculated from different datasets. The volume budget of V [Eq. (12)] is described in sec-

tion 4, where we show the importance of the different quantities B_s, D, M, A_{bnd}, and the drift of the control volume V.

3. Comparison of water mass transformations

To analyze the complete volume and buoyancy balance of the South Atlantic [Eq. (12)], we use a global high-resolution ocean model, which is described in the next section. The use of an ocean model ensures that all terms can be calculated in a consistent manner. To assess the realism of this model, we first compare the WMT $F(\sigma)$ of different datasets [see Eq. (11)]. This gives an idea of the uncertainty of the WMT and of all processes that are linked to it through the volume and buoyancy balance.

a. OCCAM

We analyze data from the high-resolution global ocean model OCCAM (Webb et al. 1997). The model uses an Arakawa-B grid and has an eddy-permitting resolution of ¼° × ¼°. The model has a free surface and 36 vertical levels at fixed depths, with 16 layers in the upper kilometer. A Laplacian horizontal diffusion and friction is used. The horizontal diffusion coefficient for tracers is 100 $m^2 s^{-1}$ and the horizontal viscosity coefficient is 200 $m^2 s^{-1}$. The Pacanowski and Philander (1981) scheme is used for the vertical mixing of tracers. Away from regions with strong shears this gives diffusivities of 0.5 $cm^2 s^{-1}$. A Laplacian vertical mixing is applied to the velocity fields with a diffusion coefficient of 1 $cm^2 s^{-1}$. The model is initialized with temperature and salinity from the Levitus datasets (Levitus et al. 1994; Levitus and Boyer 1994). The model has been run for 12 years with a spin up of 9 years. In the last 3 years six-hourly winds and wind stresses from the European Centre for Medium-Range Weather Forecasts (ECMWF; Gibson et al. 1997) have been used.

The air–sea fluxes of heat and freshwater are derived from relaxation of sea surface temperature (SST) and salinity. For the heat flux the SST dataset of Reynolds and Smith (1994) for the years 1993–95 has been used. For the freshwater flux the sea surface salinity (SSS) is relaxed to the Levitus et al. (1994) dataset. This ensures that the surface temperature and salinity cannot deviate too much from the observed values. However, the relaxation time scale of 30 days produces only a weak surface forcing and does not guarantee realistic water mass transformations (Fox and Haines 2003). The surface forcing can be divided into a part that is dependent on the temperature difference between the ocean and the atmosphere (Q_{diff}) and a part that is independent of the temperature difference (Q_{abs}). The heat flux Q_{diff} is linearly dependent on the temperature difference with climatological SST in OCCAM, while in reality this is a complex function determined by atmospheric boundary layer processes and the difference between SST and air temperature. The heat flux component Q_{abs} is not included in the OCCAM model. This will generate biases in the ocean surface temperature and the surface temperature relaxation in OCCAM cannot fully correct for this. Also, the model physics differ from real ocean physics because of subgrid-scale processes that generate model biases. Consequently, air–sea fluxes can be too large where the model has large biases, for instance the location of the Brazil–Malvinas Confluence zone and other oceanic fronts (Fox et al. 2000). But in general, relaxation to climatological SST will cause the heat fluxes to be too small as Q_{abs} is absent and Q_{diff} is smaller when the air temperature is replaced by climatological SST. Also, it is likely that a coarser model with larger mixing coefficients will constrain SST and SSS more and yield smaller fluxes. A higher resolution, more complete eddy-permitting model will have more variability and subsequently larger fluxes. Because of the relaxational forcing, the model underestimates the amplitude of SST variability and contains a lag of about one month in the seasonal cycle of SST (Fox et al. 2000). The thermocline in the OCCAM model is too diffuse. Oceanic heat transport across 30°S in the Atlantic is high in comparison with other estimates (0.63 ± 0.25 PW, see Macdonald 1998).

Water masses are transported mainly along isopycnals. This implies that, to properly describe the flow of water masses, transports should be analyzed along isopycnal surfaces. As the isopycnal spacing, or vertical density gradient, is subject to temporal variability, it is important to take into account the correlation of velocity and vertical density gradient fluctuations, defined as the bolus transport. The bolus transport does not change the vertically integrated transport, but is merely a vertical redistribution of the velocity field. For all calculations used in this study the bolus transport was included. More details of the calculation of the bolus transport and the impact on the Eulerian and Lagrangian analyses can be found in Drijfhout et al. (2003) and Donners and Drijfhout (2004).

b. Other datasets used: DaSilva, NCEP, ERA-40, and ECCO

To assess the uncertainty of WMT rates, we selected different datasets for comparison with OCCAM. It is known that fields of observed air–sea fluxes are uncertain because of the limited number of observations available, especially for the Southern Hemisphere

(Sterl 2001). Although separate terms of the volume balance can be estimated from observations, the errors are undoubtedly significant as observations in the Southern Ocean outside the summer season are sparse. Also, different turbulent flux parameterizations result in significantly different air–sea fluxes, especially under very strong and weak wind conditions (Zeng et al. 1998). We use a compilation of the Comprehensive Ocean–Atmosphere Dataset, a dataset based on in situ observations from ships and parameterizations of the air–sea interaction (henceforth DaSilva; DaSilva et al. 1994). A monthly climatology for the period from 1945 to 1993 has been used. Furthermore, the ECMWF 40-yr reanalysis (ERA-40) (Simmons and Gibson 2000) and National Centers for Environmental Prediction (NCEP) reanalysis (Kalnay et al. 1996) data have been used. Both datasets are atmospheric reanalysis products. The Estimating the Circulation and Climate of the Ocean (ECCO) dataset has been derived from the ECCO project. We used the monthly data from the 2° adjoint model (Stammer et al. 2000). For both reanalysis products and the ECCO dataset we used the period from 1992 to 1997, which overlaps the period that has been used for the forcing of the OCCAM model (1993–95).

Both reanalysis products and the DaSilva dataset have no data on the SSS. To calculate the WMT as a function of density, however, SSS is a necessary variable. We used the monthly SSS climatology from the *World Ocean Atlas 1998* (Boyer et al. 1998) for these datasets. For the ocean models OCCAM and ECCO we used the model output of SSS to calculate the WMT rates.

c. Water mass transformations

A density interval of 0.1 kg m^{-3} is used for the calculation of the transformation rate for all datasets. We use the region located from the Atlantic equator to 60°S, 70°W to 20°E. The WMT $F(\sigma)$ for all datasets is plotted in Fig. 2. A positive transformation denotes a densification of water masses by air–sea interaction. The gradient of the transformation ($\partial F/\partial\sigma$) curve denotes the amount of water mass that is formed within that particular density interval. To simplify the analysis, we also consider six water masses for the South Atlantic basin based on observational studies. The definitions are tabulated in Table 1. The formation rates for the different water masses are tabulated in Table 2. The surface water (SW) consists mainly of "Salinity Maximum Water" (Blanke et al. 2002a), which subducts in the western tropical Atlantic. Water masses with a density below $\sigma = 24.2$ are formed in the equatorial South Atlantic, primarily north of 5°S. According to Tomczak and Godfrey (1994), part of the light South Atlantic Central Water (lSACW) is Indian Central Water (ICW) brought into the South Atlantic Ocean by Agulhas Current intrusions because the temperature–salinity (T–S) curves of lSACW and ICW are virtually the same. The South Atlantic Subtropical Mode Water (SASTMW) consists of a light variety of subtropical mode waters (Provost et al. 1999), formed mainly in the Brazil Current overshoot, and 13°C mode water, presumably formed by mixing in Agulhas rings (Tomczak and Godfrey 1994). The Subantarctic Mode Water (SAMW) is formed along the subantarctic front (SAF), located between 45° and 50°S. South Atlantic Central Water (SACW) is a combination of the water masses lSACW, SASTMW, and SAMW. The Antarctic Intermediate Water (AAIW) is characterized by a salinity minimum and is formed in the eastern South Pacific and western South Atlantic (Stramma and England 1999). The oceanic heat gain along the SAF at 50°S converts AAIW into SAMW. The deep water (DW) is defined as the water mass below the AAIW. The locations of the density fronts agree closely during winter, but there is a northward bias during summer south of 40°S in the OCCAM dataset.

TABLE 1. Table with the different water masses and their definition in terms of the density interval.

Water mass	Definition
Surface water	$\sigma < 25.5$
lSACW	$25.5 < \sigma < 26.2$
SASTMW	$26.2 < \sigma < 26.6$
SAMW	$26.6 < \sigma < 27.0$
AAIW	$27.0 < \sigma < 27.3$
DW	$\sigma > 27.3$

Figure 3 shows the temperature–salinity diagram for three different locations in the South Atlantic for both the OCCAM model and the Levitus climatology. The vertical salinity gradient is weakened in the OCCAM model; while the AAIW at 30°S is too saline, the SW is too fresh. The location of the 34.2 psu contour compares well with observations (Tomczak and Godfrey 1994). The contours between 34.3 and 34.5 psu, however, are located too far south. This discrepancy can be explained by the northward bias of density fronts in the ACC, which causes an increased oceanic heat gain and evaporation. These effects compensate each other in the buoyancy flux. Farther northward the warm and salty bias of AAIW decreases and at 10°S it has almost disappeared in OCCAM (see Fig. 3). The salinity minimum is located deeper than 1100 m in the Brazil Current and the Agulhas ring corridor in the southeast Atlantic. Especially the latter may point at an overestima-

TABLE 2. Table with formation and destruction rates for different models (Sv, positive values denote water mass formation). For the datasets the standard deviation of the annual water mass formation is calculated.

Water mass	OCCAM	ECCO	ERA-40	NCEP	DaSilva
SW	−0.7 ± 6.8	−1.3 ± 7.0	−1.8 ± 5.4	−8.0 ± 3.4	−3.6
ISACW	5.6 ± 7.0	4.6 ± 7.3	−7.8 ± 4.9	6.8 ± 3.4	−0.9
SASTMW	6.0 ± 0.7	6.1 ± 4.7	10.0 ± 1.8	10.7 ± 3.8	6.6
SAMW	1.5 ± 0.8	2.4 ± 4.8	13.1 ± 3.0	11.9 ± 3.7	14.0
AAIW	−4.2 ± 0.5	−7.7 ± 3.2	−12.2 ± 1.0	−16.0 ± 1.4	−10.2
DW	−8.2 ± 1.1	−4.1 ± 0.8	−1.3 ± 0.7	−5.3 ± 1.4	−5.9

tion of the impact of Agulhas leakage on the South Atlantic in OCCAM. This might also be a reason why the salinity minimum is too salty in the extratropical South Atlantic. The SACW is slightly too fresh, especially the lSACW. This could be caused by an underestimation of evaporation in the extratropical Atlantic Ocean and a strong influx of fresher central water from the Indian Ocean. Also, the Agulhas Retroflection extends too far west and the Brazil–Malvinas Confluence Front too far south in the model. The relaxation to the Levitus dataset corrects these model biases with a spurious cooling and freshwater forcing. This might explain the cold and fresh bias of the lighter water masses in OCCAM. In general, however, there is a good qualitative agreement of the South Atlantic mode waters between OCCAM and Tomczak and Godfrey (1994).

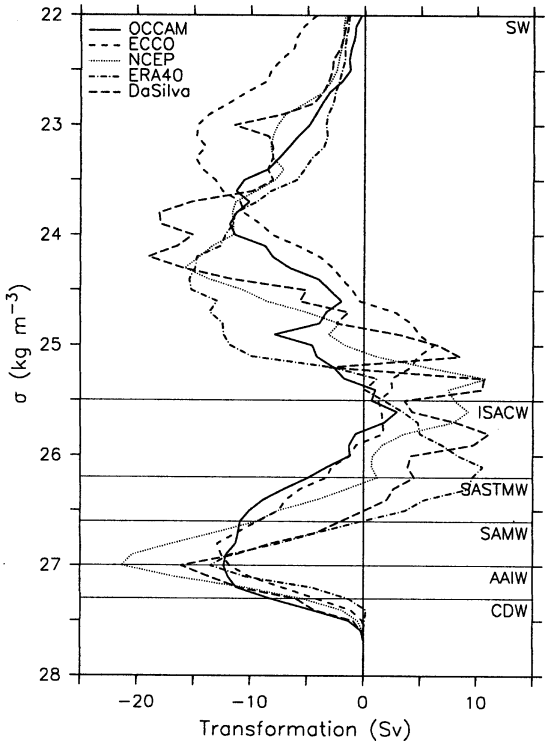

FIG. 2. Water mass transformation curves $F(\sigma)$ for the different air–sea flux datasets (Sv). Positive values denote a transformation toward higher densities.

The different datasets show a similar qualitative behavior, although the differences in formation rates are large. For light SW ($\sigma < 24.0$) the transformation is negative, while at the isopycnal level that separates SW and lSACW the transformation is positive (i.e., toward higher density) for all datasets. At the isopycnal that separates the SAMW and AAIW all datasets reach a second minimum transformation; that is, water gains buoyancy. The NCEP dataset shows a large consumption rate of SW in comparison with the other datasets. Although the seasonal cycle of the WMT of the NCEP and ERA-40 datasets agree reasonably well at this isopycnal level, the NCEP dataset is lower during 8 months. The WMT rates at the isopycnals that divide lSACW, SASTMW, SAMW, and AAIW agree closely for the ERA-40 and NCEP datasets in summer. However, the WMT rates for the ERA-40 dataset are consistently higher because of the stronger surface cooling in winter. The formation of SAMW is underestimated in both ocean-only models OCCAM and ECCO. In the OCCAM model this can be attributed to the overall weak surface forcing and its small seasonal cycle. In the ECCO model the cooling of lSACW and SASTMW is too weak in winter, while in summer the warming of AAIW is too weak in comparison with the reanalysis datasets. The datasets agree on whether there is a net formation or consumption of a particular water mass in the South Atlantic, except for lSACW. The formation rate of lSACW is uncertain because of the strong transformation of SW into lSACW in the NCEP dataset and the strong transformation of ISACW into SASTMW.

The quantitative differences in WMT rates between the datasets are approximately 10 Sv. Discrepancies could be caused either by interannual variability, uncertainties in the numerical evaluation of $F(\sigma)$, or uncertainties in the observations of heat and freshwater fluxes. The interannual variability in transformation rates has a standard deviation of 3–4 Sv and increases with density. The accuracy of the calculation method is determined by changing the density interval of the cal-

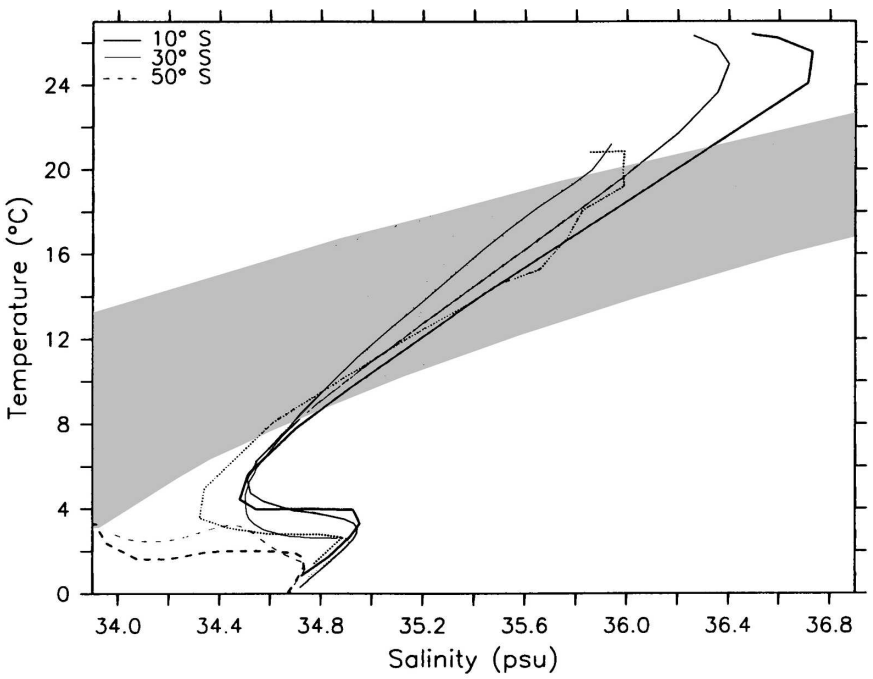

FIG. 3. The temperature–salinity diagram for three different latitudes (all at 25°W) in the South Atlantic. The thin lines are annual mean data from the OCCAM model; the thick lines are annual mean data from the Levitus climatology. The density range for the water mass SACW is indicated by the gray area.

culation of WMT. The accuracy decreases slightly with density and is on average 2 Sv. The interannual variability together with the numerical accuracy, however, cannot explain the discrepancy in WMT rates of 10 Sv between the different datasets. This discrepancy must therefore be caused by uncertainties in the observed heat and freshwater fluxes. For SW and lSACW, the uncertainties in the WMT due to heat fluxes (10 Sv) are larger than the uncertainties in the WMT due to freshwater fluxes (5 Sv). Although the uncertainty of the freshwater fluxes themselves is larger than that of the heat fluxes, the transformation rate due to heat fluxes is stronger than the transformation due to freshwater fluxes, which explains the larger uncertainty in the transformation rate. For the other water masses the uncertainty of the WMT due to heat and freshwater fluxes is similar. There is no quantitative agreement between the different datasets, assuming that the differences should be within two standard deviations.

Even though the OCCAM model uses a relaxation condition for the SST and SSS, the transformation (F) and formation ($\partial F/\partial\sigma$) rates for water masses other than SW are in good agreement with the ECCO model with data assimilation. However, the formation rates in OCCAM are weaker than for the NCEP, ERA-40, and Da Silva datasets. The OCCAM model has a broader and less strong transformation minimum (or buoyancy gain) at the isopycnal that divides SAMW and AAIW. Although the surface forcing in OCCAM could be improved, we are confident that the air–sea fluxes in OCCAM have sufficient quality to be used for this study. To be able to make a robust and quantitative estimate of transformation and formation rates, the observational dataset of air–sea fluxes needs to be improved within the South Atlantic, especially for the heat fluxes.

4. Buoyancy budget

In the previous section we showed that all datasets agree on the qualitative structure of the WMT rate due to air–sea interaction within the South Atlantic. In this section we study the total balance of the winter mixed layer in the South Atlantic for the OCCAM model. In the buoyancy budget of the winter mixed layer, five processes play an important role: air–sea interaction, trend, subduction, mixing, and interocean exchange [see Eq. (12)]. The total balance, however, is not easily determined from observations. Karstensen and Quadfasel (2002a) estimated the water mass transformation rates due to air–sea fluxes and subduction rates from observations for the three separate basins in the Southern Ocean. With these calculations the interocean exchange within the mixed layer (A_{bnd}) between the different basins in the Southern Ocean was estimated.

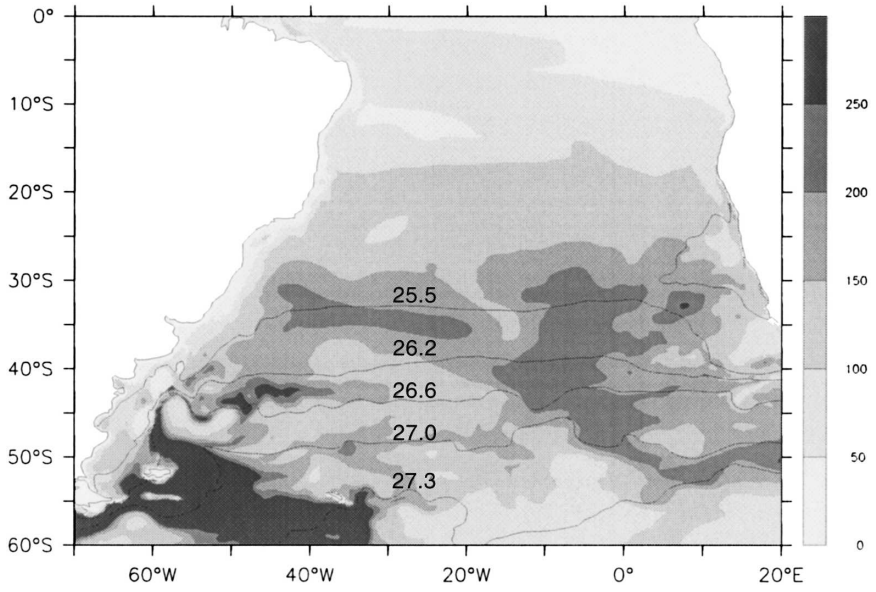

FIG. 4. Maximum mixed layer depth in OCCAM (m). The surface isopycnals that divide the outcrops of the different water masses (see Table 1) are overlaid.

However, they neglected mixing processes. With the OCCAM model we studied the volume balance in more detail. The interocean exchange A_{bnd}, Eulerian subduction M_{Eul}, and the trend in the volume of different water masses $\partial V/\partial t$ were determined explicitly, and the residual transformation must be caused by mixing processes $\partial D/\partial\sigma$.

We tried to calculate the diffusion explicitly but could not explain the residual of balance Eq. (12) for the OCCAM model. We assume that the explicit calculation of diffusion from seasonally averaged data files does not resolve the diapycnal mixing induced by internal waves that are generated by the high-frequency wind forcing (Lee et al. 2002). There was, however, a qualitative agreement. For this manuscript we used the residual of the mass balance for the diffusive term.

The OCCAM model has no explicit mixed layer scheme. Hence the mixed layer depth needs to be calculated from other properties. As a criterion we used the depth at which the density is 0.1 kg m^{-3} higher than the sea surface density. For this calculation the seasonal mean fields of temperature and salinity have been used. Because seasonal mean fields smooth out the extreme values within a season, the data were corrected with an interpolation scheme described by Killworth (1996). In Fig. 4, the deepest winter mixed layer depth is drawn together with the isopycnals separating the outcrops of the different water masses (Table 1). Karstensen and Quadfasel (2002a) showed the winter mixed layer depth calculated with a similar density criterion (0.125 kg m^{-3}) from the *World Ocean Atlas 1998* dataset, which has a quantitative agreement to the maximum mixed layer depth in OCCAM in regions with enough observations. South of 35°S and far away from the coastlines, the in situ data in winter are sparse, which makes a quantitative comparison very uncertain. Winter mixed layers are deep in the northern part of Drake Passage and in the Malvinas Current; winter mixed layers are shallow in the Cape Basin and Brazil–Malvinas Confluence regions, because of warm surface waters injected from the Agulhas Current and the Brazil Current, respectively. Talley (1999) used the depth of 95% oxygen saturation as another proxy for the winter mixed layer depth. The agreement with the OCCAM model is qualitative. Deep mixed layers (>150 m) are found at the 0° meridian between 30° and 50°S and in the Cape Basin close to the African continent winter mixed layers are shallow. The Brazil–Malvinas Confluence is a region of shallow mixed layers flanked with deep mixed layers.

We have drawn the transformation induced by each process as a function of density for the OCCAM model in Fig. 5. Figure 5a shows the balance among buoyancy input at the ocean surface (F), diffusion ($-\partial D/\partial\sigma$), trend ($\partial V/\partial t$), and the exchange with neighboring oceans and the interior ($M_{\mathrm{Eul}} + A_{\mathrm{bnd}}$). In Fig. 5b the processes responsible for the exchange with the interior and adjacent oceans are drawn separately. Negative values denote a volume flux into $V(\sigma, t)$. The decrease of the transformation over a density interval denotes a convergence of a water mass within that density range. The same results are summed for the different water

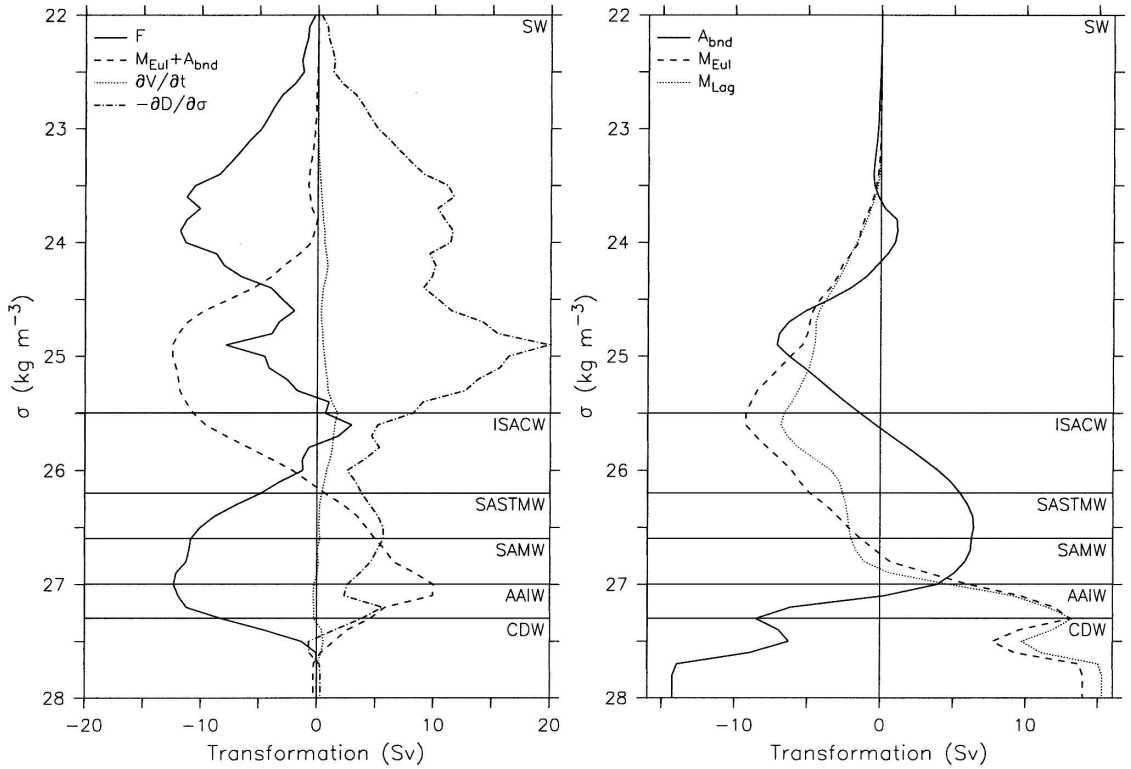

FIG. 5. (a) Transformation curve (Sv) showing the balance [(see Eq. (1)] within the domain among air–sea fluxes [$F(\sigma)$, solid]; the density-integrated, outward flux through the control surfaces [$M(\sigma) + A_{\text{bnd}}(\sigma)$, dashed]; trend (dotted); and the diffusion (dash–dotted). An increase of transformation with density denotes a loss of water from the control volume. The sum of all processes is zero because the total volume is conserved. (b) Transformation processes through the control surface: outgoing volume flux through the open boundaries: interocean exchange A_{bnd} (solid), Eulerian subduction M_{Eul} (dashed), and Lagrangian subduction M_{Lag} (dotted). The horizontal lines indicate the density bounds between different water masses (see Table 1).

masses in Fig. 6. The air–sea transformation F is negative at almost all density levels, which indicates a buoyancy gain for most water masses in the South Atlantic. The trend is a small contribution to the total buoyancy balance, but it is statistically significant. However, the average volume change of the water masses is less than 2.5% and is further neglected. Figure 5a shows that the diffusion is important, especially for the SW, and it acts to increase the density of ocean water at all levels. Down to $\sigma = 24.0$, primarily north of 12°S, formation by air–sea fluxes is completely balanced by consumption from diffusion. Niiler and Stevenson (1982) showed that turbulent vertical diffusion of heat balances surface heating in tropical oceans. For the denser SW ($24.0 < \sigma < 25.5$), in the subtropical gyre and the Agulhas region, diffusion has a strong impact on the mass balance of the control volume, mainly forming water masses heavier than $\sigma = 25.0$. Diffusion is less important for water masses, other than SW, south of the South Atlantic subtropical gyre.

The interocean exchange A_{bnd} is as large as the net subduction rate M_{Eul}. Light SW ($\sigma < 25.0$) is imported from the Indian Ocean by the Agulhas Current. The SASTMW is formed by differential heating in the STF (6.0 Sv). More than one-half of this newly formed water mass subducts (3.5 Sv). Mixing (1.7 Sv) and interocean exchange (0.8 Sv) account for the other newly formed SASTMW. The Pacific Ocean provides mainly SAMW, AAIW, and DW by the Antarctic Circumpolar Current. After transformation by air–sea interaction and mixing, these water masses either subduct or flow within the mixed layer to the Indian Ocean. All water masses except SW are exported toward the Indian Ocean (not shown). Karstensen and Quadfasel (2002a) and Sloyan and Rintoul (2001) also concluded that water formed in the South Atlantic must flow into the Indian Ocean where it finally subducts. For the mixed layer budget, the exchange between the North and South Atlantic basin is small. North Brazil Current rings play an important role in the net interhemispheric exchange and this process may be underestimated in the model. However, net exchange associated with the

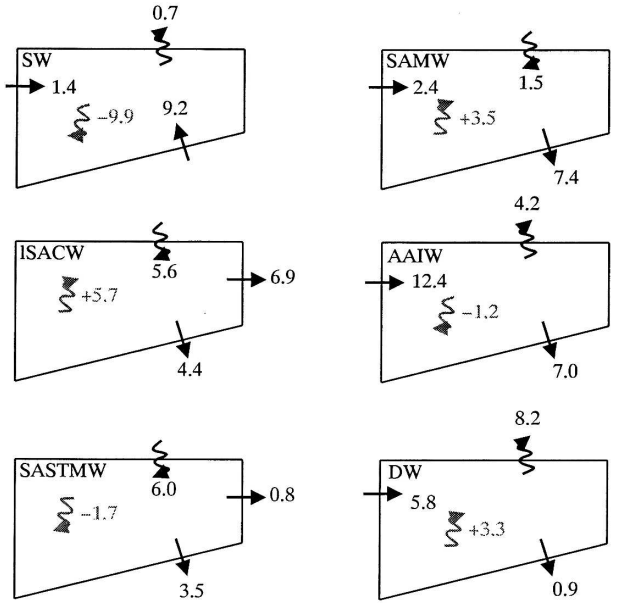

FIG. 6. Budget for four different water masses within the South Atlantic mixed layer. The different water masses are indicated by the name in the upper-left corner of each box. Water masses are defined in Table 1. All numbers are in Sverdrups. The arrows at the top of each box represent the formation from air–sea interaction. The arrows at the bottom represent the net flux across the deepest mixed layer depth. The arrows across the left or right side represent interocean exchange, whereas the arrows within the box indicate formation by mixing within the mixed layer.

THC is realistic in OCCAM. The exchange occurs predominantly below the mixed layer. The positive density-integrated subduction rate of 15 Sv at $\sigma = 28.0$ indicates that there is a net subduction of water within the South Atlantic provided by water imported from adjacent oceans. All water masses ranging from lSACW to DW subduct in the South Atlantic, while SW obducts. The Eulerian obduction of SW is located in the eastern equatorial region, the Agulhas region, and along the western boundary of the South Atlantic up to the Brazil–Malvinas Confluence area. The Lagrangian net subduction M_{Lag} has been plotted in Fig. 5b for comparison, which is further discussed in the next section. Although deviations are small, the Eulerian and Lagrangian net subduction are not equal.

5. Lagrangian connections of subduction zones

In the previous section we analyzed the volume balance of the South Atlantic mixed layer. So far, all analyses were carried out in a Eulerian framework. We have shown that the South Atlantic has a net Eulerian subduction (M_{Eul}) of more than 15 Sv in OCCAM (see Fig. 5b). This Eulerian subduction is the net mass flux across the winter mixed layer base in the South Atlantic. The Eulerian subduction does not indicate whether these water masses move in the interior ocean for more than one year nor does it give an indication of the locations that are remotely influenced by the subducted water masses. A Lagrangian analysis is needed to estimate the remote impact of subducted water masses within the South Atlantic.

The three-dimensional Lagrangian trajectory technique that we use to this end has been described and applied before (Döös 1995; Hazeleger et al. 2003; Donners and Drijfhout 2004). With Lagrangian trajectory analysis we follow particles that enter the interior ocean through the winter mixed layer base. The properties of the water masses are set in the mixed layer prior to subduction. Particles are followed until they reach the winter mixed layer base again. The properties of the mixed layer are influenced by the water masses that reenter the mixed layer. This gives an indication of possible teleconnections between South Atlantic subduction regions and remote obduction regions. Lagrangian subduction rates (S_{Lag}) are calculated by tracing forward in time, starting from the mixed layer base; while we obtain Lagrangian obduction rates (O_{Lag}) with backward time integration of particles that end at the mixed layer base.

Model drift influences the pathways of water masses below the mixed layer and consequently the obduction regions. However, we cannot directly quantify the effect of drift on the obduction regions because the Lagrangian trajectory analysis requires a dataset averaged over several years. However, we can calculate the effect of drift on Eulerian water mass transports in the OCCAM model. Donners and Drijfhout (2004) showed that the drift in meridional water mass transports in the South Atlantic in the OCCAM model is not statistically significant.

Particles represent a transport of at most 10^{-3} Sv and are evenly spread in space and time. Tens of thousands of particles have been calculated to obtain a quantitative picture of the Lagrangian subduction within the South Atlantic. The accuracy of the total transports is better than 0.1 Sv. A similar analysis for the global ocean has been done by Blanke et al. (2002b), but without distinguishing different water masses. They calculated Lagrangian trajectories between regions of subduction and obduction. We do not divide the South Atlantic into different regions, but distinguish among six water masses defined by density intervals (see Table 2).

The formation induced by air–sea interaction together with the Lagrangian subduction and reemergence zones for all water masses except DW is plotted

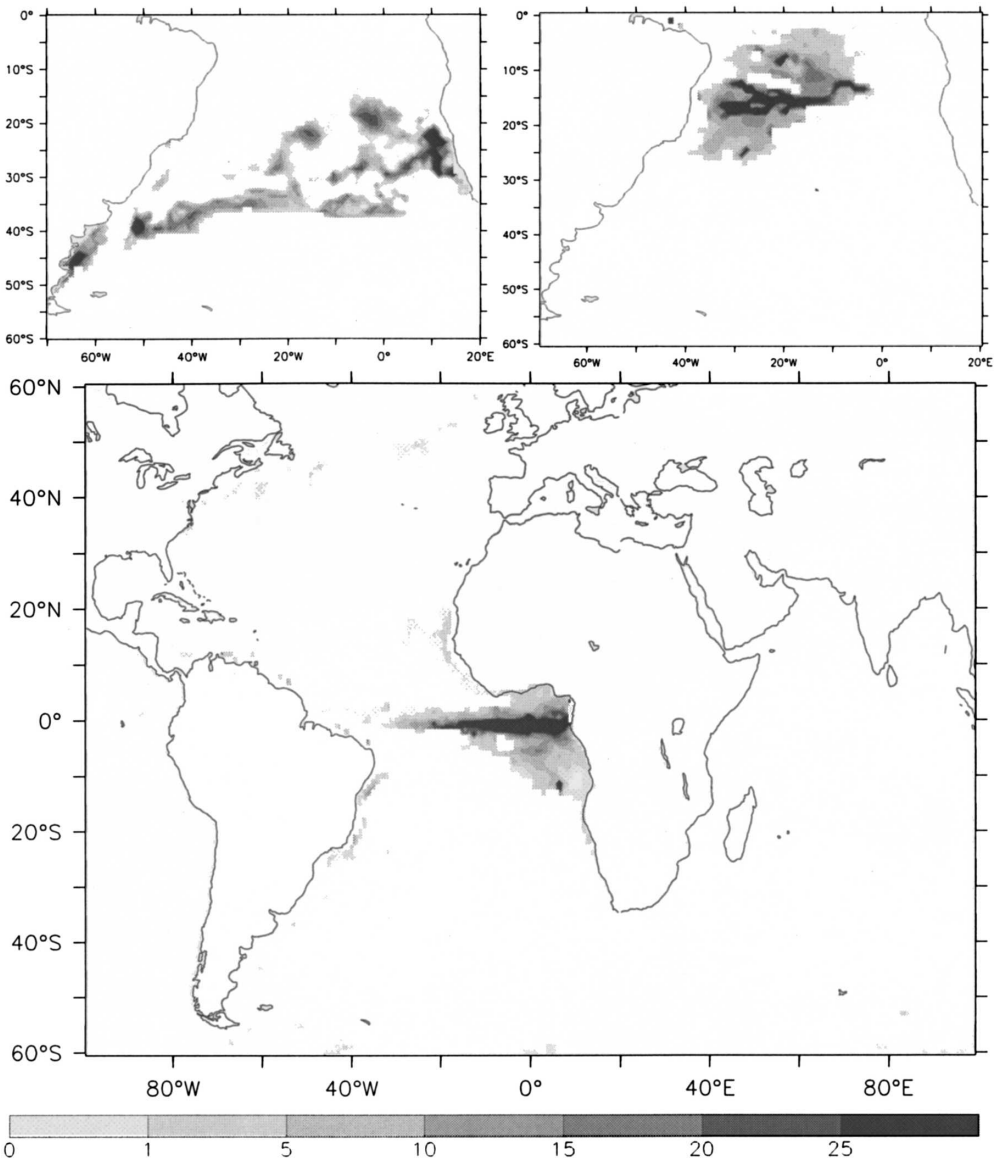

FIG. 7. (top left) Water mass formation due to air–sea fluxes together with (top right) the subduction and (bottom) reemergence regions for the SW (mSv per 1° × 1° grid box).

in Figs. 7–11. The results are quantified in Table 3. Note that the Lagrangian obduction O_{Lag} and reemergence differ because of interocean exchange: reemergence includes only particles that subducted in the South Atlantic, the Lagrangian obduction O_{Lag} includes all particles that obduct in the South Atlantic. The latter may have been subducted in the South Atlantic or in other basins. Also note that the formation is not equal to F. The formation is the integral over R of air–sea transformations that converge into a specific density class. This is an indication of the potential amount of newly formed water mass that could subduct. Formation and subduction of DW has not been plotted, as the drift of the OCCAM model for this heavy water mass could seriously hamper the Lagrangian analysis of the subduction (Lee et al. 2002), and the subduction rate of this water mass is small in the South Atlantic. There is a good, quantitative agreement with Blanke et al. (2002b). The subtropical gyre and the ACC act as the main subduction zones. The eastern equatorial upwelling regions, a strip along the western boundary, and the ACC are the main obduction zones. The median time between subduction and reemergence is less than 5 years for all water masses. Although there is no well-defined timescale for subduction, the bulk of the particles return within 7 years.

TABLE 3. Table with formation, subduction, and reemergence rates for different water masses (Sv). The reemergence of subducted water particles is divided into three different regions: tropical Atlantic (15°S–15°N), North Atlantic, and other parts of the World Ocean. The next to last column indicates that median time between subduction and reemergence (yr). The last column shows the obduction rates within the South Atlantic basin (Sv).

	Formation	S_{Lag}	Tropical Atlantic	North Atlantic	Other	Median time	O_{Lag}
SW	7.3	6.2	5.4	0.1	0.7	2.2	12.8
lSACW	14.7	12.0	4.1	0.7	7.2	3.9	8.0
SASTMW	13.0	2.8	0.4	0.2	2.2	1.9	2.2
SAMW	12.8	8.5	0.1	0.2	8.2	2.6	1.7
AAIW	9.0	13.4	0.0	0.0	13.4	4.1	5.0
DW	0.7	15.5	0.0	0.0	15.5	3.0	13.4

Figure 7 shows that SW is mainly formed by air–sea interaction in the Brazil–Malvinas Confluence, Agulhas region, and the South Atlantic Current. The subduction of SW, however, takes place in the western tropical Atlantic. This coincides with the subduction of Salinity Maximum Water (Blanke et al. 2002a). The subduction rate of SW (6.2 Sv) in OCCAM is lower than model estimes (7.2 Sv: Blanke et al. 2002a) and observational estimates (9.0 Sv: Blanke et al. 2002a). The water mass lSACW (Fig. 8) is formed along the STF and in the Cape Basin and subducts in the subtropical gyre of the South Atlantic. To reach its subduction area in the South Atlantic, a large part of the newly formed SW and ISACW has to cross the region where the curl of the wind stress vanishes, located around 30°S, and where the Ekman transport changes sign becoming southward. To overcome the Ekman drift a strong mean flow is needed to advect the SW and lSACW northward. This could be provided by the Benguela Current, which draws water from the South Atlantic Current. The connection between the two currents, however, is weak in OCCAM (Drijfhout et al. 2003). Most of the SW and lSACW formed in the South Atlantic is exported to the Indian Ocean where it recirculates and is replaced by Agulhas leakage, whereafter it subducts.

Some SASTMW is formed by cooling of lSACW, but most is formed by warming of SAMW (Fig. 9). Formation of SAMW occurs along the SAF in the ACC (Fig. 10); 12.4 Sv of AAIW is converted by surface heating into SAMW. Of the newly formed SAMW, 8.5 Sv subducts within the South Atlantic. The subducted SAMW stays within the ACC and reemerges farther downstream. Only a tiny part enters the Atlantic basin and reemerges in the Atlantic eastern equatorial region or the northern North Atlantic.

Figure 11 shows the formation areas of AAIW, which is mainly formed by buoyancy gain of cold waters south of the ACC (8.2 Sv). However, the strong transformation of light AAIW into SAMW results in a net consumption of AAIW (4.2 Sv, Fig. 11). Because of the eastward flow of the ACC, AAIW, that is subducted in the Malvinas Current and the Brazil–Malvinas confluence region, must originate from the Pacific Ocean. Newly formed AAIW partially subducts in the South Atlantic Ocean east of 20°W (0.9 Sv), but most of this AAIW is exported toward the Indian Ocean. Only a negligible part of the subducted particles reaches the northern North Atlantic. Most AAIW reemerges in the ACC downstream of the Kerguelen Plateau and in the northern part of Drake Passage. The South Atlantic mixed layer is a large net sink of AAIW, fed by AAIW from the Pacific Ocean.

6. Discussion and conclusions

a. Comparison with observations

The transformation of SAMW in the South Atlantic in OCCAM is in reasonable agreement with observations. Sloyan and Rintoul (2001) combined observations of air–sea fluxes and hydrographic sections with an inverse model to infer the ocean circulation of the Southern Hemisphere. They calculated a formation of SAMW of 8.4 Sv due to buoyancy gain of Antarctic Surface Water, as compared with an air–sea transformation of 12.4 Sv from AAIW to SAMW for the OCCAM model. The OCCAM model transforms 10.9 Sv of SAMW further into lighter SASTMW along the northern edge of the ACC. This is not in agreement with inverse model calculations, based on the DaSilva dataset, that show an opposite transformation of 6 Sv due to enhanced heat and freshwater loss of thermocline water in the Brazil–Malvinas Confluence (Sloyan and Rintoul 2001). However, Karstensen and Quadfasel (2002a) used the NCEP dataset and calculated similar transformation rates as the OCCAM model at this density. This can also be seen in Fig. 2, with comparable WMT rates for OCCAM, ECCO, and NCEP, whereas the DaSilva and ERA-40 datasets show almost no WMT at the $\sigma = 26.6$ isopycnal. This shows the need to improve datasets for air–sea fluxes.

The transformation rate at the isopycnal $\sigma = 26.2$ has

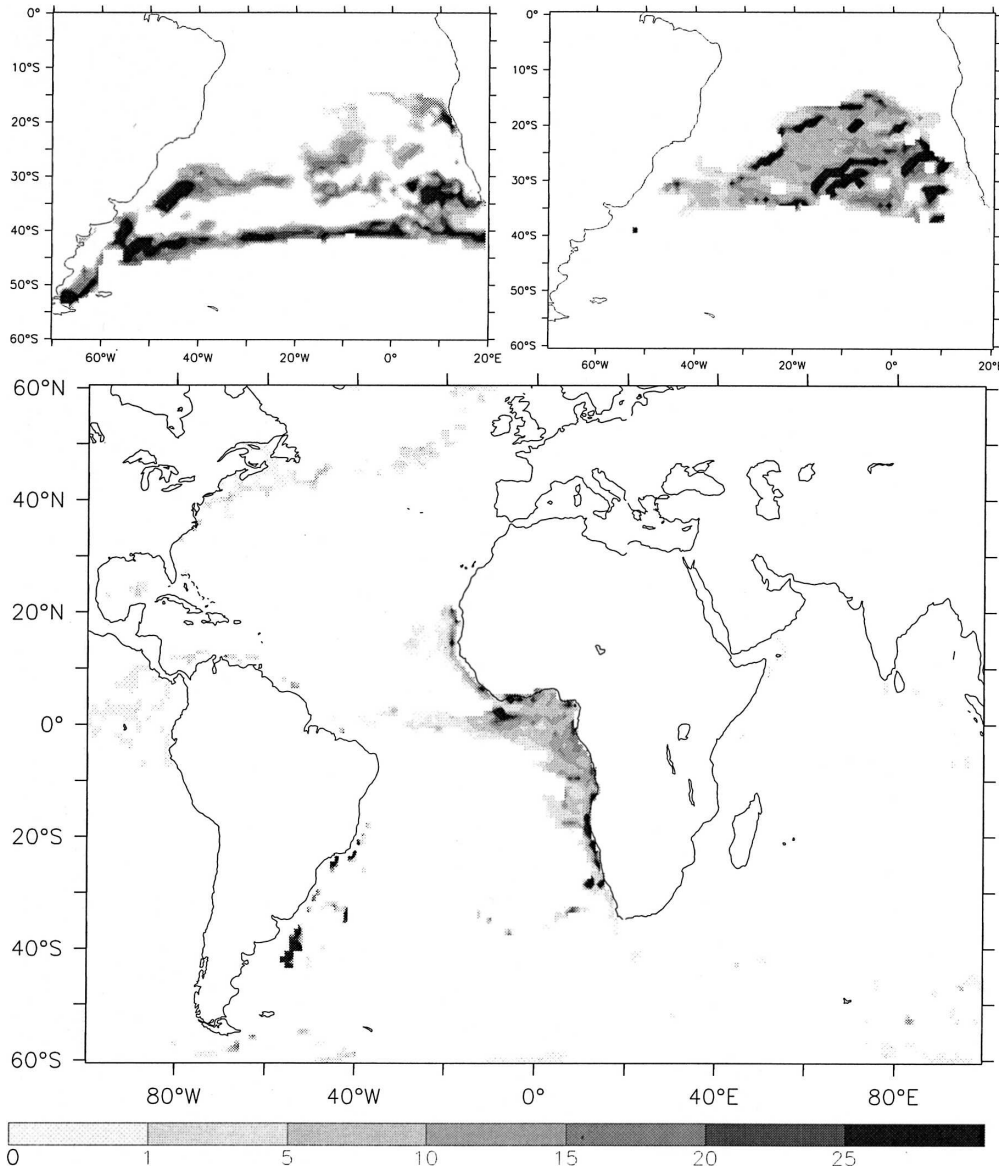

FIG. 8. As in Fig. 7 but for the lSACW.

an even larger uncertainty (Fig. 2). Ocean-only models (OCCAM and ECCO) transform SASTMW to lSACW, while for all other datasets the reverse transformation takes place. The STF in the OCCAM model is northward biased during summer, which leads to more heat input. This results in a negative bias of the WMT rate in OCCAM. The high variability of SW and lSACW formation rates (see Table 3) indicates that a longer period is needed for a meaningful estimate of average formation rates at these densities.

Poole and Tomczak (1999) separated SACW into Eastern SACW (ESACW) and Western SACW (WSACW). The ESACW represents thermocline waters transferred into the Atlantic Ocean at the Agulhas Retroflection; WSACW is locally subducted in the subtropical convergence. Poole and Tomczak (1999) showed that the WSACW dominated the South Atlantic at shallow depths (300 m). Of the total SACW formation of 20.6 Sv by air–sea interaction and mixing in the OCCAM model, 75% subducts. In agreement with Poole and Tomczak (1999), the subducted lSACW resides mostly within the Atlantic basin (10.5 Sv), while subducted SAMW does not penetrate the Atlantic basin farther northward. Furthermore, Donners and Drijfhout (2004) showed that, in the OCCAM model, all ESACW is (9.5 Sv) directly transported toward the

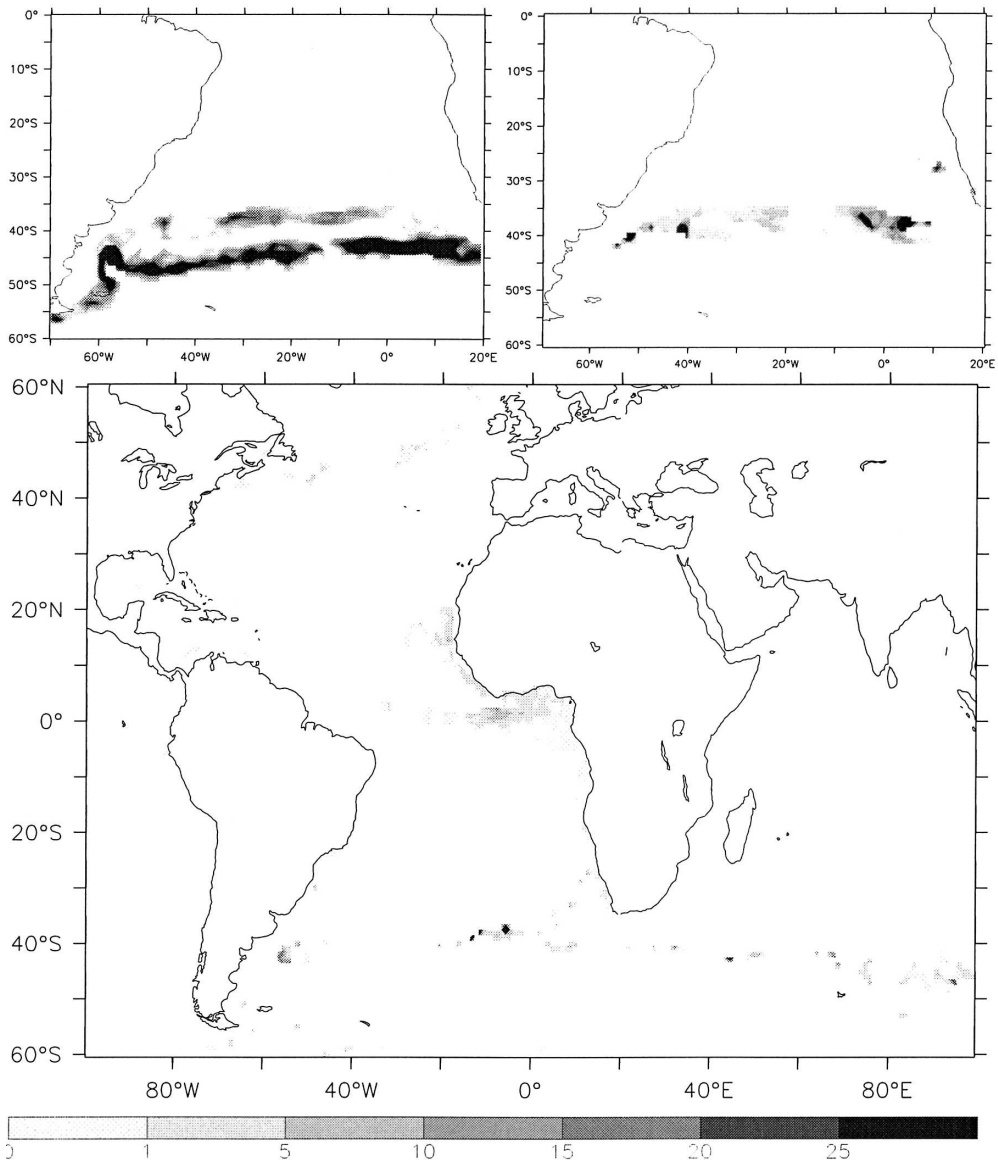

FIG. 9. As in Fig. 7 but for the SASTMW.

North Atlantic, dominating the tropical Atlantic SACW at deeper depths.

The AAIW layer of the South Atlantic has been extensively described by Talley (1996) and Sloyan and Rintoul (2001). There are two distinct formation regions for AAIW: the southwestern Atlantic and the southeastern Pacific. A large volume of Pacific AAIW is formed by strong cooling of SAMW in the southeastern Pacific. This formation region serves the northward AAIW transport in the Pacific and feeds the South Atlantic with AAIW that enters through Drake Passage. This AAIW subducts as South Atlantic AAIW along the Malvinas Current. In OCCAM, over 12.6 Sv of AAIW subducts in the Malvinas Current. This AAIW must be drawn from Drake Passage, in accordance with observations, because AAIW formation in the South Atlantic is located farther downstream.

Karstensen and Quadfasel (2002a) estimated the water mass formation due to air–sea fluxes and the subduction rate for the Southern Hemisphere from observational data. Their conclusions are radically different from the ones we obtain from OCCAM. Karstensen and Quadfasel (2002a) added all water masses with densities between $\sigma = 25.2$ and $\sigma = 27.0$ together. The subduction rate calculated by Karstensen and Quadfasel (2002a) is 21 Sv, which is stronger than the subduction rate in the OCCAM model (13.8 Sv). Also the formation rate calculated by Karstensen and Quadfasel

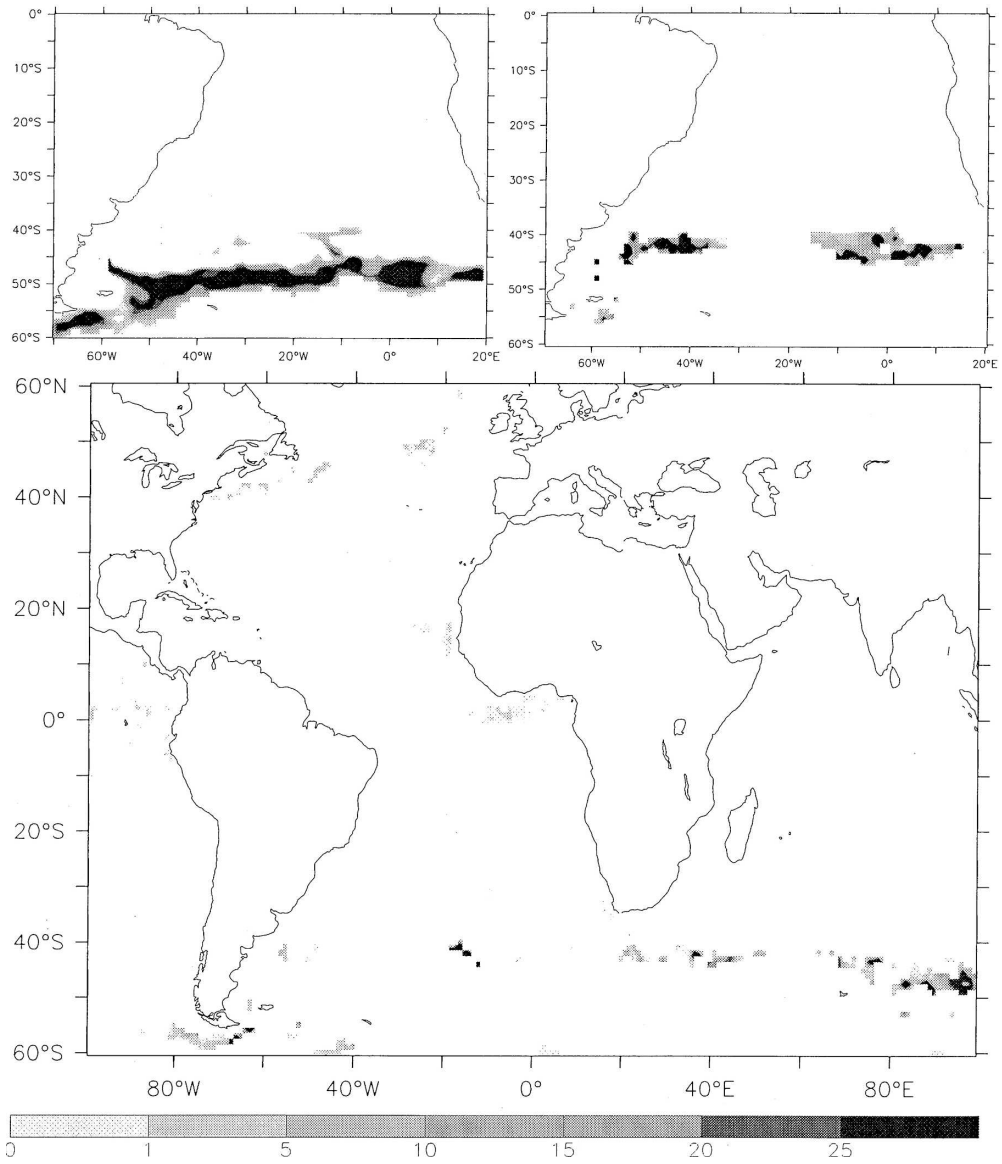

FIG. 10. As in Fig. 7 but for the SAMW.

(2002a) is much larger than calculated for the OCCAM model (29 Sv versus 9.7 Sv). One of the causes for this large discrepancy could be the surface relaxation used by the OCCAM model, which underestimates the water mass transformation rates. Also, Karstensen and Quadfasel (2002a) used the NCEP air–sea flux dataset, which has the strongest formation rate for this density range (see Fig. 2). There is, however, some agreement on the interocean exchange between the South Atlantic and Indian Oceans. Karstensen and Quadfasel (2002a) estimated 13 Sv of water to be exported, while the OCCAM model shows an export of 8.2 Sv. To accommodate this export, 12.3 Sv is provided by diffusive processes in the OCCAM model. This shows that, at least for the OCCAM model, diffusive processes cannot be ignored to estimate the interocean exchange. However, the water-mass transformation F can be used to qualitatively estimate the sum of interocean exchange and Eulerian subduction ($M_{\mathrm{Eul}} + A_{\mathrm{bnd}}$); the error is on average 80%.

b. *Impact of the South Atlantic on the properties of the upper branch of the THC*

So far, we have analyzed the water mass transformation and exchange in the South Atlantic mixed layer. With Lagrangian trajectory analysis the fate of subducted water masses has been calculated. The impact of these water mass transformations in the South Atlantic

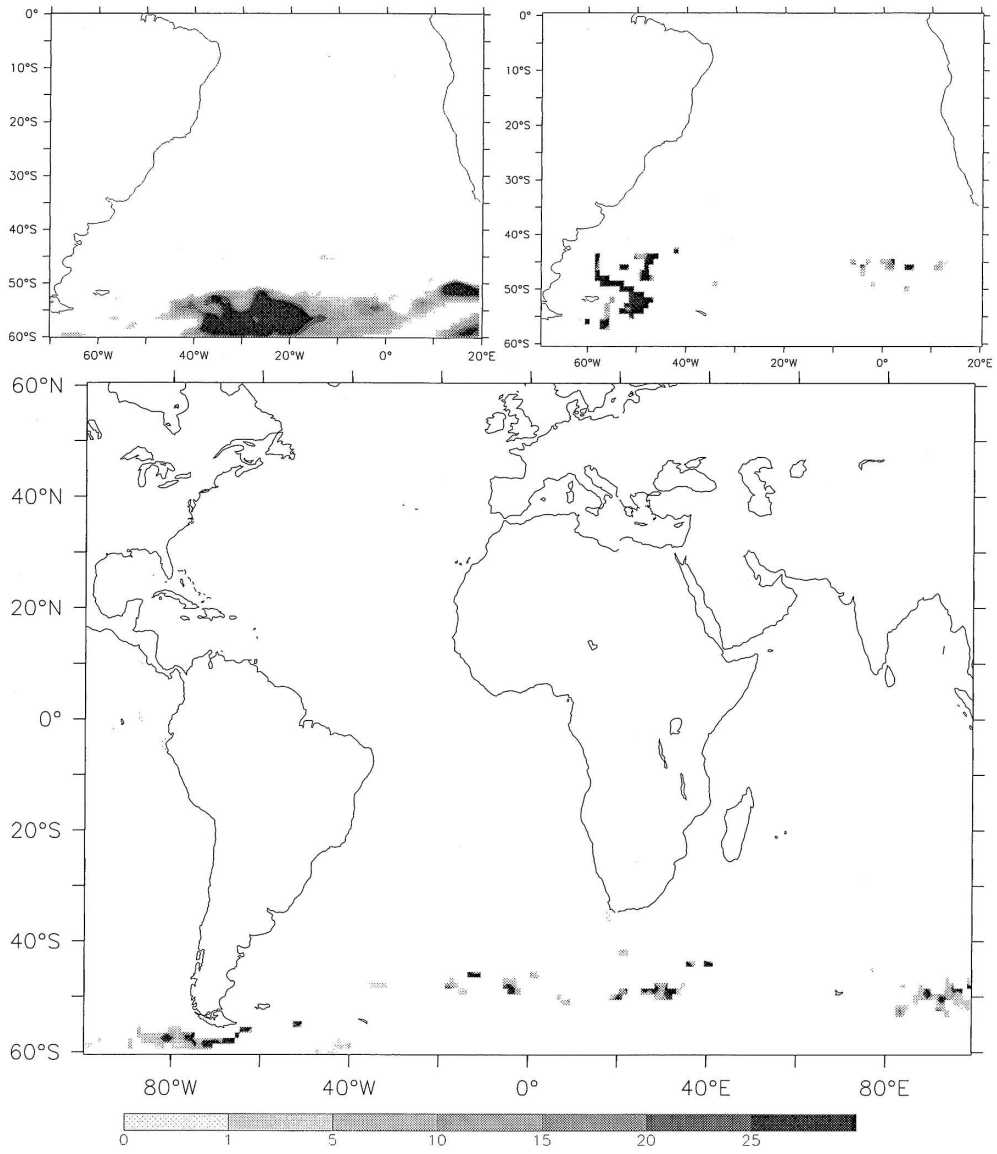

FIG. 11. As in Fig. 7 but for the AAIW.

Ocean on the thermohaline overturning circulation, however, is not directly apparent from these calculations. With the same Lagrangian methodology we can also calculate the impact of South Atlantic mixed layer processes on the upper branch of the thermohaline circulation. To this end, we follow particles at the Atlantic equator below the mixed layer backward in time to the point where they enter the Indo–Atlantic basin from the Pacific (Speich et al. 2001). This enables us to single out the transformations of the water that is part of the meridional overturning circulation.

Here 14.4 Sv enters the Indo–Atlantic basin from the Pacific Ocean and crosses the Atlantic equator northwards. These water masses are modified within the Indo–Atlantic basin, both in the mixed layer and below the mixed layer. A large part subducts for the last time in the South Atlantic basin (6.9 Sv, not shown) before crossing the equator. Water-mass transformations and mixing in the South Atlantic thus have a significant impact on the upper branch of the THC. In Fig. 12 we show the transformation in the South Atlantic of the transport crossing the Atlantic equator. The upper branch of the THC is transformed at all density levels in the South Atlantic Ocean. The water masses with a density $\sigma < 26.0$ lose buoyancy because of strong surface cooling in the Agulhas region. Surface warming along the ACC increases the buoyancy of Antarctic intermediate and mode waters ($\sigma > 26.0$). The THC

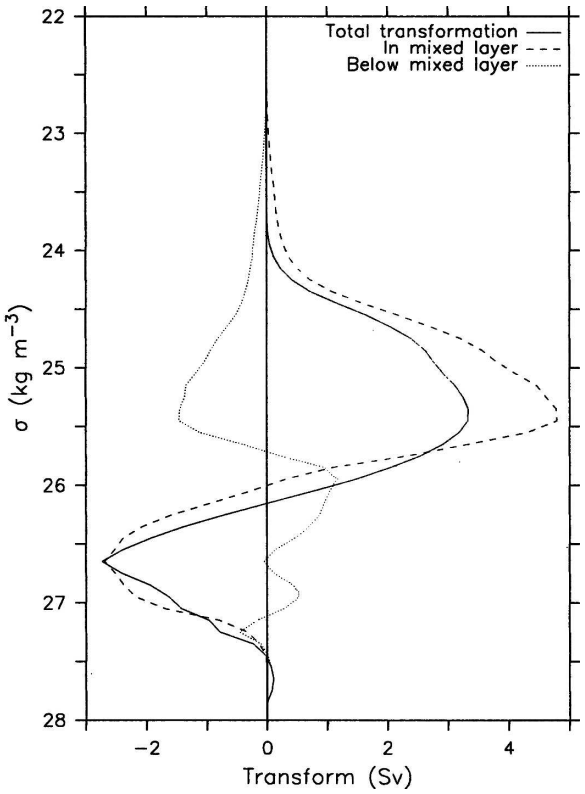

FIG. 12. Water mass transformation curves of the upper branch of the THC in the South Atlantic (Sv). The total transformation is plotted with the solid line. The total transformation is split into two components: the transformation in the mixed layer (dashed) and the transformation below the mixed layer (dotted). A positive transformation denotes densification.

gains buoyancy below the mixed layer for $\sigma = 25.5$ in the eastern tropical Atlantic.

The subducted transport from the South Atlantic into the North Atlantic does not necessarily influence directly the deep-water formation in the northern North Atlantic. A large part (3.0 Sv) of the subducted water particles reemerge within the tropical Atlantic (15°S–15°N), where the water mass properties can again be modified by mixed layer processes. Only 1.1 Sv of the water subducted in the South Atlantic connects directly to reemergence areas in the northern north Atlantic. All other transport recirculates back into the South Atlantic, to reemerge somewhere else.

The following picture emerges from these calculations: there is a strong teleconnection between the South and tropical Atlantic, and this also applies to the upper branch of the THC. A majority of the water involved in NADW formation is also ventilated in the tropical and subtropical North Atlantic. A direct teleconnection between the subpolar North Atlantic and areas remote from the tropical Atlantic applies to no more than 50% of the NADW return flow. A direct teleconnection between the northern North Atlantic and the South Atlantic applies to only 1 Sv of the THC.

c. *Conclusions*

We calculated WMT rates for the South Atlantic due to air–sea fluxes for different datasets, ranging from observation-only datasets to model-only datasets. The datasets are in qualitative agreement, although the deviations of the transformation rates for the different datasets are 10 Sv. The air–sea interaction in the OCCAM model supplies buoyancy to the South Atlantic at all density levels. Heavy water masses (AAIW and DW) are transformed into lighter water masses (SASTMW and SAMW). Diffusion generally counteracts the air–sea interaction by extracting buoyancy from the mixed layer. Because of diffusion, water mass formation rates calculated from air–sea heat and freshwater fluxes are ineffective to estimate of the sum of Eulerian subduction rates and interocean exchange.

The subduction of water masses within the South Atlantic has been analyzed with Lagrangian trajectory analysis. The subducted water masses reemerge at remote locations and this generates teleconnections by pathways through the interior ocean. The Subantarctic Mmode Water and Antarctic Intermediate Water that subducts in the South Atlantic flows farther eastward along the ACC, where it finally reemerges and is further modified. This implies that these water masses can only provide the NADW return flow by an indirect pathway, first looping into other basins. Part of the lighter water masses flow directly to the North Atlantic. But most of these subtropical water masses reemerge in the eastern tropical Atlantic, while a minor part reemerges along the eastern boundary or the Brazil–Malvinas Confluence. This indicates that there is a teleconnection through the interior ocean between the South Atlantic subtropics and Tropics. Only 1.2 Sv of subducted water in the South Atlantic crosses the Atlantic equator and reemerges in the subtropical or northern North Atlantic. This indicates that there is only a weak teleconnection between the extratropical regions of the North and South Atlantic. The direct influence of subducted water masses from the South Atlantic on the THC is therefore small. On the other hand, part of the NADW return flow is significantly transformed when crossing the South Atlantic.

Acknowledgments. The research presented in this paper is supported by the Research Council for Earth and Life Sciences (ALW) of the Netherlands Organisation for Scientific Research (NWO), and is part of the MARE project and the CLIVARNET program. The

manuscript benefited strongly from the remarks of the reviewers. The Ingrid Web site of the IRI has been used to download several datasets. We used the software package Ferret for all plots in this manuscript.

APPENDIX

Symbols Used in Text

σ	potential density anomaly (kg m^{-3})
t	time (s)
R	region of interest
$H(x, y)$	deepest mixed layer within R (m)
$V(\sigma, t)$	volume of water with a density lower than σ, bounded by the region of interest, the deepest mixed layer, and the sea surface (m^3)
$M(\sigma, t)$	volume flux from $V(\sigma, t)$ into the interior ocean ($m^3\ s^{-1}$)
$A_{bnd}(\sigma, t)$	volume flux from $V(\sigma, t)$ to adjacent basins ($m^3\ s^{-1}$)
$A(\sigma, t)$	diapycnal volume flux across isopycnal σ within $H(x, y)$, positive for flow toward increasing σ ($m^3\ s^{-1}$)
$B(\sigma, t)$	total buoyancy loss of $V(\sigma, t)$ (kg s^{-1})
$B_s(\sigma, t)$	buoyancy loss through the sea surface of $V(\sigma, t)$ (kg s^{-1})
$D(\sigma, t)$	diffusion across bounding surface of $V(\sigma, t)$ (kg s^{-1})

REFERENCES

Blanke, B., M. Arhan, A. Lazar, and G. Prévost, 2002a: A Lagrangian numerical investigation of the origins and fates of the Salinity Maximum Water in the Atlantic. *J. Geophys. Res.,* **107,** 3163, doi:10.1029/2002JC001318.

——, S. Speich, G. Madec, and R. Maugé, 2002b: A global diagnostic of interior ocean ventilation. *Geophys. Res. Lett.,* **29,** 1267, doi:10.1029/2001GL013727.

Boyer, T. P., S. Levitus, J. I. Antoniv, M. E. Conkright, T. D. O'Brien, and C. Stephens, 1998: *Salinity of the Atlantic Ocean*. Vol. 4, *World Ocean Atlas 1998*, NOAA Atlas NESDIS 30, 166 pp.

Cushman-Roisin, B., 1987: Subduction. *Dynamics of the Oceanic Surface Mixed Layer: Proc. 'Aha Huliko'a Hawaiian Winter Workshop,* Honolulu, HI, University of Hawaii at Manoa, 181–196.

DaSilva, A. M., C. C. Young, and S. Levitus, 1994: *Algorithms and Procedures*. Vol. 1, *Atlas of Surface Marine Data,* NOAA Atlas NESDIS 6, 74 pp.

Donners, J., and S. Drijfhout, 2004: The Lagrangian view of South Atlantic interocean exchange in a global ocean model compared with inverse model results. *J. Phys. Oceanogr.,* **34,** 1019–1035.

Döös, K., 1995: Interocean exchange of water masses. *J. Geophys. Res.,* **100,** 13 499–13 514.

Drijfhout, S. S., P. de Vries, K. Döös, and A. C. Coward, 2003: Impact of eddy-induced transport on the Lagrangian structure of the upper branch of the thermohaline circulation. *J. Phys. Oceanogr.,* **33,** 2141–2155.

Fox, A. D., and K. Haines, 2003: Interpretation of water mass transformations diagnosed from data assimilation. *J. Phys. Oceanogr.,* **33,** 485–498.

——, ——, B. A. de Cuevas, and D. J. Webb, 2000: Altimeter assimilation in the OCCAM global model, Part II: TOPEX/Poseidon and *ERS-1* assimilation. *J. Mar. Syst.,* **26,** 323–347.

Gibson, R., P. Kållberg, S. Uppala, A. Hernandez, A. Nomura, and E. Serrano, 1997: 1997: The ERA description, the ECMWF re-analysis project report series. ECMWF Tech. Rep. 1, 77 pp.

Gnanadesikan, A., and H. W. Hallberg, 2000: On the relationship of the circumpolar current to Southern Hemisphere winds in coarse-resolution ocean models. *J. Phys. Oceanogr.,* **30,** 2013–2034.

Hazeleger, W., P. de Vries, and Y. Friocourt, 2003: Sources of the Equatorial Undercurrent in the Atlantic in a high-resolution ocean model. *J. Phys. Oceanogr.,* **33,** 677–693.

Kalnay, E., and Coauthors, 1996: The NCEP/NCAR 40-Year Reanalysis Project. *Bull. Amer. Meteor. Soc.,* **77,** 437–471.

Karstensen, J., and D. Quadfasel, 2002a: Formation of Southern Hemisphere thermocline waters: Water mass conversion and subduction. *J. Phys. Oceanogr.,* **32,** 3020–3038.

——, and ——, 2002b: Water subducted into the Indian Ocean subtropical gyre. *Deep-Sea Res.,* **49B,** 1441–1457.

Killworth, P. D., 1996: Time interpolation of forcing fields in ocean models. *J. Phys. Oceanogr.,* **26,** 136–143.

Lee, M.-M., A. C. Coward, and A. G. Nurser, 2002: Spurious diapycnal mixing of the deep waters in an eddy-permitting global ocean model. *J. Phys. Oceanogr.,* **32,** 9–99.

Levitus, S., and T. P. Boyer, 1994: *Temperature.* Vol. 4, *World Ocean Atlas 1994,* NOAA Atlas NESDIS 4, 117 pp.

——, R. Burgett, and T. P. Boyer, 1994: *Salinity*. Vol. 3, *World Ocean Atlas,* NOAA Atlas NESDIS 3, 99 pp.

Macdonald, A. M., 1998: The global ocean circulation: A hydrographic estimate and regional analysis. *Progress in Oceanography,* Vol. 41, Pergamon, 281–382.

Marshall, J. C., D. Olbers, H. Ross, and D. Wolf-Gladrow, 1993: Potential vorticity contraints on the dynamics and hydrography of the Southern Ocean. *J. Phys. Oceanogr.,* **23,** 465–487.

——, D. Jamous, and J. Nilsson, 1999: Reconciling thermodynamic and dynamic methods of computation of water-mass transformation rates. *Deep-Sea Res.,* **46A,** 545–572.

Niiler, P., and J. Stevenson, 1982: The heat budget of tropical ocean warm-water pools. *J. Mar. Res.,* **40** (Suppl.), 465–480.

Nurser, A. J. G., R. Marsh, and R. G. Williams, 1999: Diagnosing water mass formation from air–sea fluxes and surface mixing. *J. Phys. Oceanogr.,* **29,** 1468–1487.

Pacanowski, R. C., and S. G. H. Philander, 1981: Parameterization of vertical mixing in numerical models of tropical oceans. *J. Phys. Oceanogr.,* **11,** 1443–1451.

Poole, R., and M. Tomczak, 1999: Optimum multiparameter analysis of the water mass structure in the Atlantic Ocean thermocline. *Deep-Sea Res.,* **46A,** 1895–1921.

Provost, C., C. Escoffier, K. Maamaatuaiahutapu, A. Kartavtseff, and V. Garon, 1999: Subtropical mode waters in the South Atlantic Ocean. *J. Geophys. Res.,* **104,** 21 033–21 049.

Qiu, B., and R. X. Huang, 1995: Ventilation of the North Atlantic and North Pacific: Subduction versus obduction. *J. Phys. Oceanogr.,* **25,** 2374–2390.

Reynolds, R. W., and T. M. Smith, 1994: Improved global sea sur-

face temperature analyses using optimal interpolation. *J. Climate,* **7,** 929–948.

Simmons, A. J., and J. K. Gibson, 2000: The ERA-40 project plan: ERA-40 project report series. ECMWF Tech. Rep. 1, 63 pp.

Sloyan, B. M., and S. R. Rintoul, 2001: Circulation, renewal and modification of Antarctic mode and intermediate water. *J. Phys. Oceanogr.,* **31,** 1005–1030.

Speer, K., and E. Tziperman, 1992: Rates of water mass formation in the North Atlantic Ocean. *J. Phys. Oceanogr.,* **22,** 93–104.

——, H.-J. Isemer, and A. Biastoch, 1995: Water mass formation from revised COADS data. *J. Phys. Oceanogr.,* **25,** 2444–2457.

Speich, S., B. Blanke, and G. Madec, 2001: Warm and cold water routes of an O.G.C.M. thermohaline conveyor belt. *Geophys. Res. Lett.,* **28,** 311–314.

Stammer, D., and Coauthors, 2000: The global ocean state during 1992–1997 estimated from ocean observations and a global circulation model, Part I: Methodology and estimated state. Scripps Institution of Oceanography Tech. Rep. 4, 53 pp.

Sterl, A., 2001: On the impact of gap-filling algorithms on variability patterns of reconstructed oceanic surface fields. *Geophys. Res. Lett.,* **28,** 2473–2476.

Stramma, L., and M. England, 1999: On the water masses and mean circulation of the South Atlantic Ocean. *J. Geophys. Res.,* **104,** 20 863–20 883.

Talley, L. D., 1996: Antarctic intermediate water in the South Atlantic. *The South Atlantic: Present and Past Circulation*, G. Wefer et al., Eds., Springer-Verlag, 219–238.

——, 1999: Some aspects of ocean heat transport by the shallow, intermediate and deep overturning circulations. *Mechanisms of Global Climate Change at Millennial Time Scales,* P. Clark et al., Eds., Amer. Geophys. Union, 1–22.

Tomczak, M., and J. S. Godfrey, 1994: *Regional Oceanography: An Introduction.* Pergamon, 390 pp.

Tziperman, E., 1986: On the role of interior mixing and air–sea fluxes in determining the stratification and circulation of the oceans. *J. Phys. Oceanogr.,* **16,** 680–693.

Walin, G., 1982: On the relation between sea-surface heat flow and thermal circulation in the ocean. *Tellus,* **34,** 187–195.

Webb, D. J., A. C. Coward, B. de Cuevas, and C. S. Gwilliam, 1997: A multiprocessor ocean general circulation model using message passing. *J. Atmos. Oceanic Technol.,* **14,** 175–183.

Weijer, W., W. P. M. de Ruijter, A. Sterl, and S. S. Drijfhout, 2002: Response of the Atlantic overturning circulation to South Atlantic sources of buoyancy. *Global Planet. Change,* **34,** 292–311.

Zeng, X., M. Zhao, and R. E. Dickinson, 1998: Intercomparison of bulk aerodynamic algorithms for the computation of sea surface fluxes using TOGA COARE and TAO data. *J. Climate,* **11,** 2628–2644.